Performance Analysis of a Modified Savonius Rotor Using a Variable Blade Thickness

Mohanad Al-Ghriybah
Department of Renewable Energy Engineering, Faculty of Engineering, Isra University

https://doi.org/10.5109/4842522

出版情報：Evergreen. 9 (3), pp.645-653, 2022-09. 九州大学グリーンテクノロジー研究教育センター
バージョン：

Performance Analysis of a Modified Savonius Rotor Using a Variable Blade Thickness

Mohanad Al-Ghriybah[1,*]

[1]Department of Renewable Energy Engineering, Faculty of Engineering, Isra University, Amman-Jordan

*Author to whom correspondence should be addressed:
E-mail: Mohanad.alghriybah@iu.edu.jo

(Received May 21, 2022; Revised June 21, 2022; accepted July 16, 2022).

Abstract: Wind power is one of the green energies that could be used for meeting these energy demands. This is attributed to the fact that such a source of power is free and widely available. Savonius wind rotor can work at low wind speeds which fits well the rural areas. Despite its cheap, robust, and simple design, the Savonius rotor has some negatives such as relatively low efficiency and high fluctuations of static torque. Given this, the main goal of this research is to improve the output power of the Savonius wind rotor by varying the blade thickness using numerical simulation. Investigation methods based on the rotational speed of the rotor tip, wind field characterizations, torque, and power coefficients are conducted. The K-Ɛ/realizable model was utilized for simulating the rotor at 9 m/s wind speed via Ansys Fluent software. Results demonstrate that the newly-developed rotor with varying blade thickness has a less wind wake on the internal surface of the returning blade. Moreover, the suction vortices have a higher velocity for the new configuration causing a reduction in pressure on the outer side of the returning rotor which indicates less negative torque. Compared with the traditional Savonius blades, the new model shows a 40% performance enhancement in the maximum power coefficient. The maximum power coefficient is found to be 0.20. This configuration can be useful for small-scale electricity generation in urban areas.

Keywords: Savonius; Wind power; VAWT; Wind turbine

1. Introduction

The formation of conventional energy resources such as natural gas, oil, and coal requires many years. These types of fuel cannot be formed as fast as they are being consumed[1)]. Moreover, in the coming few years, harvesting such fuel will turn out to be environmentally damaging and costly. Consequently, moving from conventional energy generation toward green and renewable energy generation approaches is an essential challenge for researchers[2)]. Renewable energy including wind, solar, and hydraulic energies contributed about 27.3% to the global overall electricity generation at the end of 2019 and it is estimated to be around 40%% by the end of 2030[3)]. The global continuous growth of the renewable energy sector is producing a green energy revolution that can be more reliable in the current decade. Hence, there are worthy opportunities for the countries and the energy industries that will invest in improving, trading, and manufacturing green technologies for producing energy[3)].

Among green energy sources, wind energy is considered a dominant clean and renewable energy source of its sustainability, availability, and cost-effectiveness[4,5)]. Wind energy covers about 4% of world electricity and it is the globe's fastest-growing source of renewable energy[6)]. The gross capacity of the global wind energy generation was about 651 Gw at the end of 2019 with an annual increase of about 10% compared to the previous year 2018. This capacity was able to cover around 6% of the worldwide electricity demand[7)]. Wind turbines family could be classified into two main sections based on the orientation of the shaft, i.e. the horizontal axis wind turbine (HAWT) where the rotational axis is in the same direction of the flow, and the vertical axis wind turbine (VAWT) in which the wind direction is perpendicular to the axis of rotation[8,9)]. HAWT is the most efficient kind of wind turbine due to its great aerodynamics[10,11)]. However, this type of turbine is not applicable for capturing wind energy in regions with less turbulent winds such as urban areas[12)]. On the other hand, VAWT has some features over the HAWT such as cost-effectiveness, the ability to produce power regardless of wind direction, and the low levels of noise, these features promote the VAWT as the best choice for the cities and isolated regions[13)].

VAWT category can be classified into two main sub-classes depending on the working force i.e. lift-force rotors (Darrieus wind rotor) and drag-force rotors (Savonius wind rotor)[14,15)]. Savonius rotor is the simplest design among the VAWT family, it mainly consists of two

blades with a semi-curricular profile shape that is attached to a vertical central shaft. The rotational movement of the Savonius rotor is generated by the difference in pressure between the advancing blade (blade with a cupped side that spins in the same direction of the wind flow) and the returning blade (blade with a rounded side that moves against the wind flow). As the point where the resultant of these two pressure (positive pressure from the advancing blade and opposite pressure from the returning blade) is not located sideways with the rotational axis, mechanical torque is produced to start the spinning of the rotor[16].

Research relevance to the Savonius wind rotor has been growing rapidly in the last decade considering its simple design, low construction cost, independence of wind direction, self-starting ability, ease of maintenance, and noiselessness[17-20]. However, this style of turbine has some drawbacks such as low power coefficient and large fluctuations of torque as a result of negative instantaneous torque at certain azimuth angles.

Based on these drawbacks, numerous studies aimed to improve the efficiency of this rotor by changing the main design parameters. The impact of using multi-stages on the efficiency of the Savonius wind machine was evaluated by Kamoji et al.[21]. The authors investigated the performance of single, double, and triple stages turbines. It was concluded that the single-stage turbine offers a higher power coefficient (Cp) compared to the double and triple-stage turbines. Nevertheless, the torque fluctuations are reduced by rising stages number. Hayashi et al.[22] performed an experimental study on the conventional Savonius rotor with one stage and modified Savonius turbine with three stages. The outcomes of the research showed that the variation in the dynamic and static torque coefficients over a full rotation (360°) of the modified rotor with three stages is positive at all the azimuth angles compared to the conventional rotor with a single stage. Based on the aspect ratio of the rotor (the ratio between the height and the diameter of the rotor) several studies had been conducted to raise the efficiency of the rotor. Mahmoud et al.[23] performed an experimental investigation using different ratios of aspect ratio (from 0.5 to 5). Their outcomes illustrated that the power coefficient was improved by raising the value of the aspect ratio. Modi et al.[24] concluded that the 0.77 aspect ratio gives the highest efficiency for the Savonius turbine. On the other hand, researchers studied the effect of adding some simple accessories called end plates at both ends of the rotor[25]. They concluded that the endplates were able to raise the performance of the rotor by preventing the leakage of the air from inward curves to the exterior flow managing the pressure difference at a favorable level over the rotor height. Numerous researches have been carried out aiming to rise the aerodynamic efficiency of the turbine with the use of power augmentations devices such as wind deflectors, guide vanes, and curtains[26]. The studies were further extended in terms of changing the overlap ratio (ratio of the gap between the blades and the turbine diameter). Akwa et al[27] performed a numerical simulation on the effect of overlap ratio by considering different values between 0 and 0.6. The results concluded that the rotor with 0.15 has the best performance among the tested rotors. Additionally, numerical studies are carried out aiming to study the effect of the supplementary internal blades on the performance of the conventional Savonius wind rotor[28,29]. The results illustrated that the power coefficient can reach 0.1885 when the inner blade is positioned at the middle position with an angle of 120° and can reach an enhancement of 32.9% when the distance between the supplementary inner blades is changed to 0.005 m.

Innovations in blade profile optimization have been carried out in abundant studies. Bach-type profile was investigated resulting in a higher power coefficient (9% more than the conventional semi-circular profile) at an overlap ratio in the range of 0 to 0.3[30]. Rahai and Hefazi[31] examined the effect of the Benesh-type profile on the performance of the Savonius rotor and concluded that using such an arrangement results in a higher power coefficient up to 0.31. Banerjee et al.[32] examined the performance of the Savonius wind turbine using an elliptical profile and found an improvement in the generated power by about 11% compared to the conventional semi-circular profile. A new blade profile has been developed by Roy and Saha[33], and Roy et al.,[34] called the modified Bach profile. This rotor was able to perform better than the conventional rotor with a maximum power coefficient of (Cp_{max} = 0.39). Saha et al.[35] found the maximum power coefficient of a twisted bladed turbine to be at a twist angle of 15°. Zhang et al.[36] conducted a numerical investigation on the arc-blade of the Savonius wind rotor using an optimization equation. Results revealed that the power coefficient was 10.98% more than the basic Savonius rotor. Consequently, over the past decades, different blade profiles and designs have been developed aiming to increase the efficiency of the turbine. Nonetheless, the geometrical parameters have been varied in these investigations. However, no research focuses on the variable thickness of the blade (the thickness of the blade increases from the blade tip to the centerline of the blade). Based on that, the current study aims to analyze numerically the performance of a modified profile of the traditional Savonius turbine by using a blade with variable thickness.

2. Physical geometry

In the present investigation, a modified Savonius rotor utilizing a variable blade thickness is proposed instead of the conventional rotor with fixed blade thickness, and its performance is investigated using a numerical simulation approach. The proposed rotor is shown in figure 1.

The base of the blade is drawn with a diameter of 0.188 m. Then three lines are constructed on the tip of the blade (L1), the root of the blade (L2), and the center of the blade (L3) with values of 0.02 m, 0.02 m, and 0.07 m,

respectively. An arc with three points has been constructed between the ends of the three lines which gives the final shape of the blade with a variable thickness. The final geometry of the rotor compared to the conventional rotor is illustrated in Figure 2. According to the figure, (d) represents the blade diameter, (D) represents the main diameter of the rotor, and e represents the shaft diameter. Both the conventional and the modified rotors are subjected to a uniform flow with a velocity of V = 9 m/s and spin with an angular speed of (ω). Both rotors have a diameter of (D = 0.442 m), and a shaft diameter (e = 0.03m).

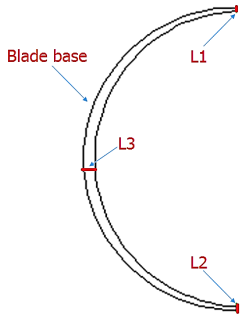

Fig. 1: Proposed blade

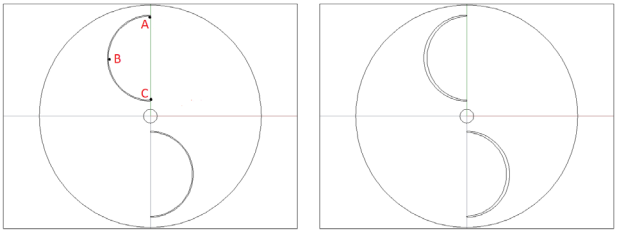

Fig. 2: (a) conventional rotor, (b) proposed rotor

3. Numerical and mathematical formulation

In the current research, a simulation based on 2D analysis is done utilizing the commercial Ansys Fluent 2021 R1. The fluent solver has the advantage of solving flow problems around complex geometries and models at a low cost. Additionally, the Savonius models were modeled utilizing the commercial software AutoCAD version 2013.

3.1 Governing equations

As the airflow near the Savonius wind turbine is unsteady, turbulent, and incompressible, the RANS (Reynolds Averaged Navier-Stokes) scheme is used here because it has high accuracy and a relatively low computational cost. The conservative equations can be expressed as follows[37]:

•Continuity equation:

$$\frac{\partial}{\partial x_i}(\bar{u}_i + \acute{u}_i) = 0 \qquad (1)$$

Where $\bar{u}_i$ refers to the prevailing wind speed, $\acute{u}_i$ is the velocity variations under the influence of turbulence, and x is the direction of the prevailing wind.

•Momentum equation:

$$\frac{\partial \bar{u}_i}{\partial t} + \bar{u}_j \frac{\partial \bar{u}_i}{\partial x_j} = -\frac{1}{\rho}\frac{\partial \bar{p}}{\partial x_i} + \frac{\mu}{\rho}\frac{\partial^2 \bar{u}_i}{\partial x_i \partial x_j} - \frac{\partial}{\partial x_j}\overline{u_i' u_j'} \qquad (2)$$

Wherein ρ is the averaged pressure, t is the time, μ is the fluid dynamic viscosity, and ρ is the fluid density.

Moreover, the realizable (k-ε) turbulent model has been selected in this research. This model has a couple of equations; one equation is used for considering K (the specific turbulent kinetic energy) and the other equation is used for considering ε (the specific turbulent dissipation rate). These equations are illustrated below:

$$\frac{\partial(\rho k)}{\partial t} + \frac{\partial(\rho k u_j)}{\partial x_j} = \frac{\partial\left(\left(\mu + \frac{\mu_t}{\sigma_k}\right)\frac{\partial k}{\partial x_j}\right)}{\partial x_j} + G_k + G_b - \rho\varepsilon - Y_M + S_k \qquad (3)$$

$$\frac{\partial(\rho\varepsilon)}{\partial t} + \frac{\partial(\rho\varepsilon u_j)}{\partial x_j} = \frac{\partial\left(\left(\mu + \frac{\mu_t}{\sigma_\varepsilon}\right)\frac{\partial \varepsilon}{\partial x_j}\right)}{\partial x_j} + \rho C_1 S_\varepsilon - \rho C_2 \frac{\varepsilon^2}{k + \sqrt{v\varepsilon}} + C_{1\varepsilon}\frac{\varepsilon}{k} C_3 G_b + S_\varepsilon \qquad (4)$$

Wherein μ_t represents the eddy viscosity, $(\sigma_k, \sigma_\varepsilon)$ are the diffusion constants, and $C_1 = \max\left[0.43, \frac{\eta}{\eta+5}\right], \eta = S\frac{k}{\varepsilon}, S = \sqrt{2S_{ij}S_{ij}}$.

The input values of constants are illustrated in Table 1.

Table 1. Constant input values.

Parameter	Value
C_1	1.44
C	1.9
σ_k	1
σ_ε	1.2

3.2 Numerical domain and boundary conditions

Figure 3 illustrates the two-dimensional scheme of the adopted numerical domain through the present investigation. The main domain is square-shaped. The size of the main domain is taken as 10 times the main turbine diameter. The main idea behind selecting a large domain is to reduce the influence of the domain boundaries on the effectiveness of the rotating turbine. Due to the large domain, the influence of the boundaries on the turbine's output power is diminished and the effect of the blockage ratio is neglected. The main domain is split into two sub-domains, a circular moving sub-domain that holds the rotor models, and a rectangular stationary sub-domain that represents the wind tunnel. An interface between the two sub-domains was introduced to assist in transferring the data of the flow during the simulations. The center of the turbine is placed midway through the squared domain (i.e. 5D from the top side of the domain and 5D from the bottom wall of the domain). The left side of the domain represents the inlet of the flow, the right side represents the flow outlet, and the sides represent the domain walls. A no-slip condition has been assumed around the surfaces of the blades. Air with a velocity of 9 m/s has been set at

the entrance of the domain. A TSR with numerous values ranging from 0.2 to 0.7 were selected in order to define the rotation of the circular sub-domain utilizing the sliding mesh.

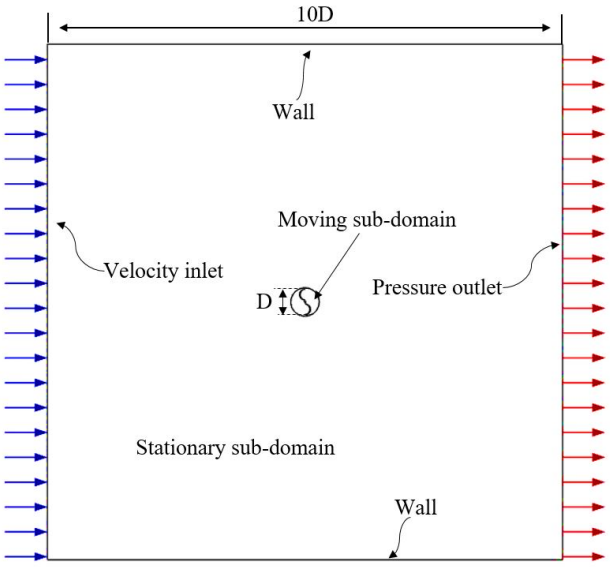

Fig. 3: Layout of the computational domain

3.3 Meshing

The grid generation was carried out utilizing the built-in mechanical mesh in the Ansys software. A quadrilateral grid with unstructured mesh was created around the squared sub-domain. Whereas the circular rotating sub-domain has a finer mesh than that used for the stationary sub-domain in order to give a more accurate solution of the flow around the turbine blades. Inflations with 25 layers and a growth ratio of 1.10 were generated on the outer surface of the rotors to be able to consider the boundary layer effect around the blades' walls. Refinement with a grade of 3 was generated on the interface between the stationary and the rotating domains aiming to improve the adaption of the blade geometry. Figures 4, 5, and 6 show the final generated mesh of all the domains and the inflations on the outer surface of the rotors.

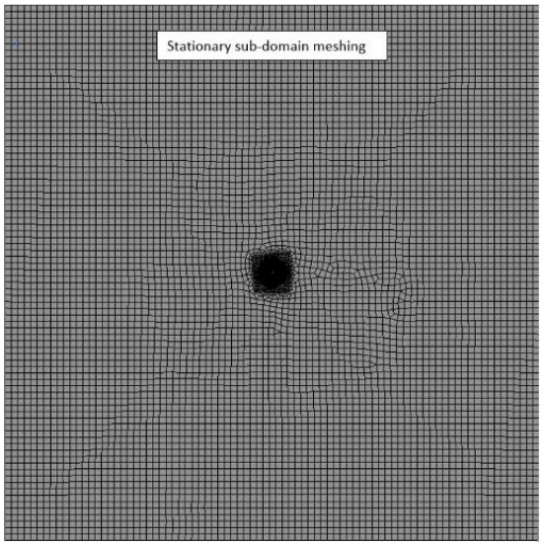

Fig. 4: Stationary sub-domain meshing

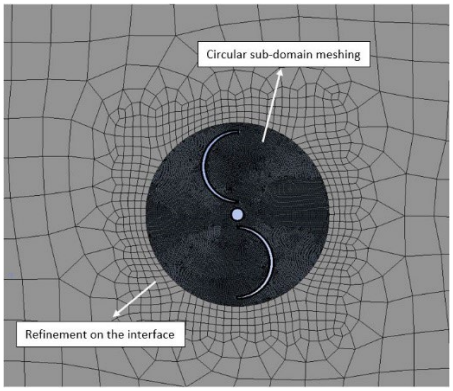

Fig. 5: Circular sub-domain meshing

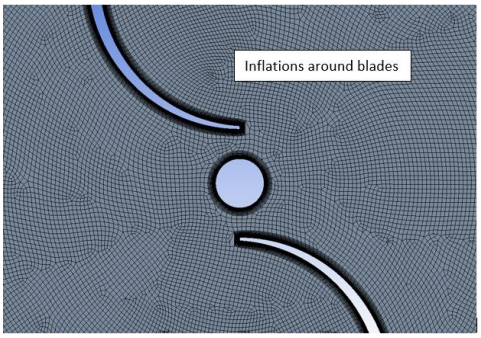

Fig. 6: Inflations around the rotor

3.4 Settings of the fluent solver

Airflow near the Savonius wind turbine was numerically simulated utilizing an unsteady as the interaction between the air and the surface of the rotors is transient. The Navier-Stokes equation was solved utilizing the realizable k- ε turbulence model where this model has been commonly utilized in the Savonius turbine studies. Additionally, this model is suitable for estimating the wall function coefficient in an accurate form more than the other models.

A transient setting was chosen in the main setting of the fluent solver. The SIMPLE algorithm was utilized for the coupling between the pressure and the velocity. The

spinning of the model was produced using the sliding mesh. Rotors are set to rotate with an azimuth angle of 5° for each time step. Ten full rotations (0° - 360°) were adopted for each rotor in order to raise the accuracy of the output results. The time steps were set to be 720 with 20 iterations for each time step to ensure that the residuals were small enough.

3.5 Performance parameters

Tip-Speed-Ratio (TSR) is considered one of the significant parameters that can be utilized to characterize the variables influencing the efficiency of the Savonius wind turbine. This parameter represents the ratio between the rotational speed of the tip of the turbine blades (u) to the wind velocity (V) and it can be expressed as follows:

$$TSR = \frac{u}{V} \qquad (5)$$

Savonius rotor performance is usually described by the ratio of the actual produced mechanical power to the available power in the wind and is called the coefficient of power (Cp) and it is defined as:

$$Cp = \frac{T \times \omega}{0.5 \times \rho \times A \times V^3} \qquad (6)$$

Where A refers to the area of the turbine and it can be expressed as turbine height × turbine diameter, T is the generated torque from the turbine spinning.

The ratio between the generated torque by the turbine and the actual torque can be defined as the coefficient of torque (Ct) which can be expressed as follows:

$$Ct = \frac{T}{0.25 \times \rho \times V^2 \times A \times D} \qquad (7)$$

Where D is the rotor diameter.

Coefficients of torque and power can be linked using the below equation:

$$Cp = TSR \times Ct \qquad (8)$$

4. Results and discussion

4.1 Grid-independent test

With the purpose of ensuring highly precise results and reducing the numerical simulation cost and time, a grid-independent test has to be conducted to choose the suitable size of the mesh. In this investigation, the grid-independent test has been conducted using three various grids. The first one (fine mesh) has 223,415 elements, the second grid (medium mesh) has 130,813 elements, and the third grid (coarse grid) has 62,583 elements. It can be observed from Table 2 that the coefficient of power of the first and second grids is almost the same which reflects the fact that the efficiency of the rotor is not affected by rising element of the grid more than 130,813, hence, the second mesh with 130,813 elements is considered for the current numerical simulations to save the time and cost of the process.

Table 2. Cp vs. mesh type.

Mesh type	Elements number	Cp
1st grid (Fine mesh)	223,415	0.1256
2nd grid (Medium mesh)	130,813	0.1247
3rd grid (Coarse mesh)	62,583	0.0912

4.2 Numerical Model validation

In this investigation, the accuracy of the numerical model of the Savonius wind rotor is evaluated depending on the experimental results of Hayashi et al.[22]. Therefore, the conventional Savonius geometry is opted from the study and used to validate the current numerical model. The represented results in Figure 7 illustrate that the average relative errors between the simulation and the experimental data are less than 7%. Consequently, the high precision of the numerical model is confirmed to be dependable and could be utilized for further simulations.

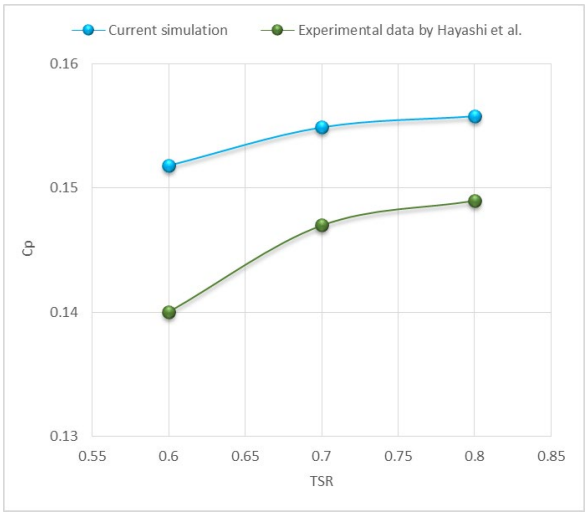

Fig. 7: Numerical model validation

4.3 Power and torque coefficients comparison

A two-dimensional simulation is performed on the newly developed and conventional Savonius rotors. A thorough assessment of the power coefficient (Cp) for both rotors is shown in Figure 8, where Cp is found to be higher in the newly developed model than in the conventional model at all the tested values of TSR. The general trend of the Cp curve for both rotors is almost the same where the Cp value starts increasing at TSR = 0.2 until reaches the maximum value of Cp at TSR = 0.4 and then decreases until reaches the lowest value at TSR = 0.7. Additionally, it can be seen from the Cp curve that the proposed blade has a greater Cp improvement at the high values of TSR (TSR > 0.3). The maximum Cp value for the proposed Savonius turbine is found to be about 0.20 at 0.4 TSR, while, at a similar value of TSR, the efficiency of the basic model of the Savonius turbine is found to be less than the proposed rotor with a value of Cp = 0.16 which illustrates an enhancement of 26.7% for the newly developed rotor. Moreover, a maximum improvement of 40% can be noticed at the maximum considered value of

TSR = 0.7. Additionally, it can be observed from the figure that the results of the current modification are better than the proposed rotor by Mosbahi et al.[38] in terms of Cp.

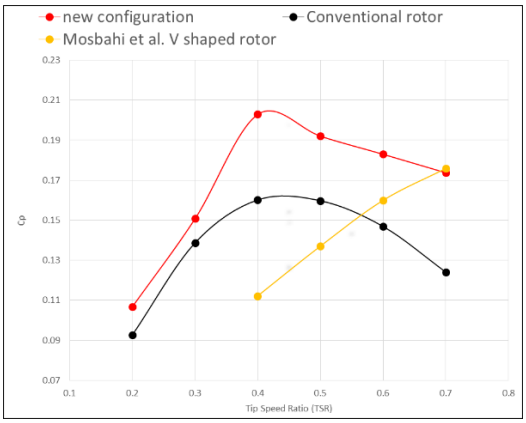

Fig. 8: Cp for the newly developed configuration vs the conventional rotor and rotor by Mosbahi et al.[38]

A comparison between the averaged values of the torque coefficient (Ct) for the proposed and conventional rotors is shown in Figure 9. It can be noticed from the curves that the averaged Ct of the proposed rotor is higher at all the TSR points. Moreover, The Ct values of both profiles decrease with TSR increase. This phenomenon is attributed to the fact that the rotation speed of the turbine minimize with load application and hence, the Ct decreases with the increase of TSR. The maximum value of Ct is about 0.534 at tip speed ratio (TSR = 0.2) for the proposed geometry whereas the conventional rotor has a value of 0.463 at the same TSR.

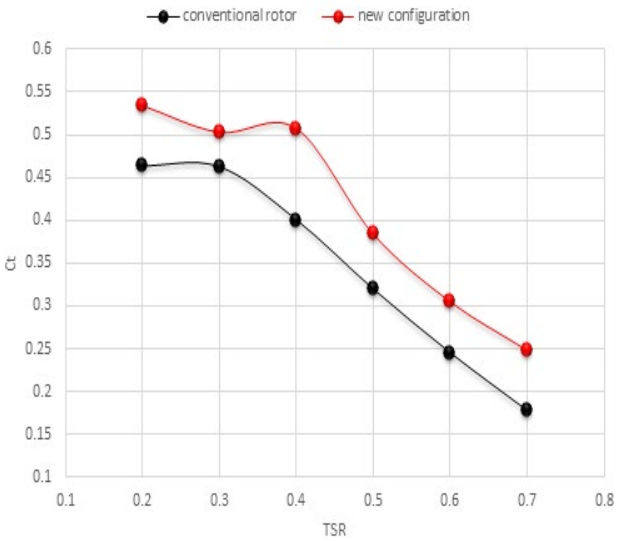

Fig. 9: Ct for the newly developed configuration vs the conventional rotor

Figures 10 and 11 illustrate the instantaneous variations of Ct of the proposed and the conventional rotors in a full rotation period (0° - 360°) and at tip speed ratios of TSR = 0.3 and TSR = 0.7, respectively. Ct curves illustrate that the instantaneous torque consists of two cycles in one full spin. Additionally, the instantaneous Ct is improved, especially at the rotational angle between (140° – 240°) at TSR = 0.3, and between (0° – 120°) at TSR = 0.7. The maximum value of Ct for the new configuration is generated at an angle of rotation equal to 85° with a value of 0.734 at TSR = 0.3, whereas the maximum Ct for the same configuration is generated at an angle of 90° at TSR = 0.7 with a value of 0.683. Additionally, it can be observed from Figure 11 that the new configuration was able to eliminate the effect of the negative torque at the high values of TSR, especially in the regions between (0° – 45°) and (210° – 220°) which explains the gain in the performance of the rotor.

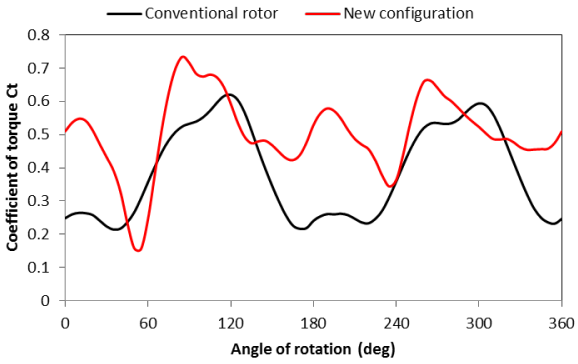

Fig. 10: Instantaneous Ct for the conventional rotor vs the newly developed configuration at TSR = 0.3

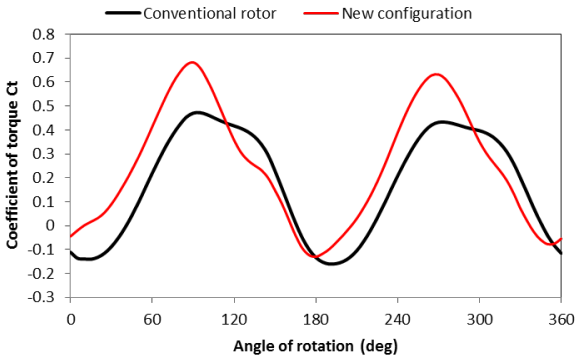

Fig. 11: Instantaneous Ct for the conventional rotor vs the newly developed configuration at TSR = 0.7

4.4 Pressure contours

The distribution of the air pressure around both (the conventional Savonius rotor and the new configuration) is illustrated to study the flow characteristic around the blades, as illustrated in Figure 12. In order to provide a better illustration, the pressure contours at three different rotation angles (30°, 90°, and 240°) are chosen at TSR = 0.7 for both rotors. At the rotor azimuth angle of 30°, a lower pressure area can be observed behind the edge of the advancing blade which indicates a lower resistance

between the blade and the airflow. Moreover, it can be noticed that the cupped side of the advancing rotor has a higher pressure in the case of the new configuration compared to the basic conventional rotor. These two factors lead to a higher positive torque to spin the blades. At the rotor azimuth angle of 90°, a great low pressure appears outside of the advancing blade (at the rounded side of the blade) which contributes to decreasing the negative torque of the blade. At an azimuth angle of 240°, higher pressure can be observed at both the cupped side of the returning and advancing blades which also increases the net positive pressure. As a general observation, it can be seen that there are high fluctuations in the generated pressure around the blades leading to high levels of turbulence for the basic style of Savonius turbine as compared to the newly developed profile showing an improvement in terms of torque of the later.

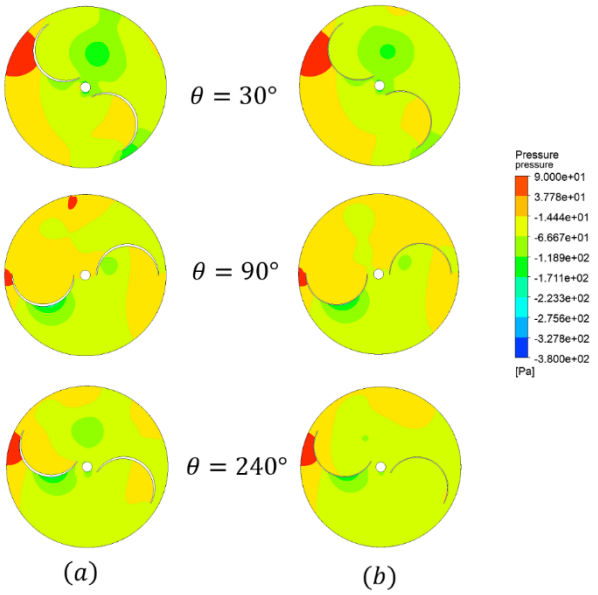

Fig. 12: Contours of pressure distribution for (a) new configuration, (b) conventional rotor

4.5 Velocity contours

The velocity contour of both rotors is shown in Figure 13. The velocity around the surface of the newly developed rotor was noticed to be between 3 and 7 m/s, whereas the velocity for the conventional rotor ranges between 2 – 4 m/s. Wake formations on the inner surface of the returning blade of the conventional rotor are found to be greater than the new rotor. Moreover, the outer surface of the returning side of the new rotor has a smaller velocity region which indicates less negative torque as compared to the conventional rotor. This shows a higher power coefficient of the new model. Additionally, the enhanced overlapping flow is noticed in the new model compared to the conventional rotor. Hence, the efficiency of the new model is greater than the conventional basic model.

4.6 Streamlines

The velocity streamlines contours are shown in Figure 14. It can be seen from the contours that the new model has higher speed suction vortices which decrease the total pressure around the outer side of the returning rotor. Additionally, the reverse flow is higher in the case of the new configuration, causing a pressure reduction on the inner surface of the advancing blade. This enhancement is attributed to the new curvatures of the blades resulting from varying the blade thickness which eases the passing of the upstream flow between the tip and the root of the blades.

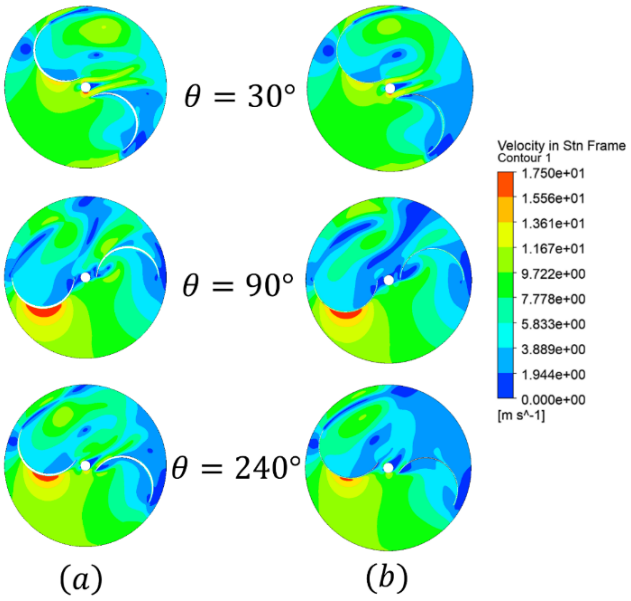

Fig. 13: Contours of the air velocity for (a) new configuration, (b) conventional rotor

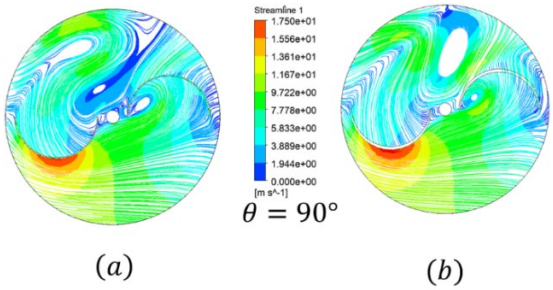

Fig. 14: Velocity streamlines contours for (a) conventional rotor, (b) new configuration

5. Conclusions

The current study evaluated the Savonius rotor performance enhancement at 9 m/s wind speed utilizing a blade with a variable thickness compared to the traditional Savonius turbine at different values of TSR using a numerical simulation. The new model has lower wake formations on the inner surface of the returning blade compared to the conventional model. Moreover, the outer surface of the returning blade has a smaller velocity region

which indicates less negative torque as compared to the traditional Savonius blades. Moreover, the new configuration has a higher reverse flow, resulting in minimizing the pressure generated on the inner surface of the advancing blade. This shows an enhancement in the power coefficient of the new profile. This enhancement is due to the new curvatures of the blades resulting from varying the blade thickness which eases the passing of the upstream flow between the tip and the root of the blades. A maximum improvement of 40% can be noticed at the highest value of TSR = 0.7. This configuration can be useful for small-scale electricity generation in urban areas.

References

1) D. Icaza, D. Borge-Diez, and S. P. Galindo, "Proposal of 100% renewable energy production for the City of Cuenca- Ecuador by 2050," Renew. Energy, vol. 170, pp. 1324–1341, Jun. 2021.
2) F. Jelti, A. Allouhi, M. S. Büker, R. Saadani, and A. Jamil, "Renewable Power Generation: A Supply Chain Perspective," Sustainability, vol. 13, no. 3, p. 1271, Jan. 2021.
3) REN21, "Renewables Global Status Report," 2020.
4) M. Al-Ghriybah, Z. Fadhli, D. Hissein, and S. Mohd, "Wind energy assessment for the capital city of Jordan, Amman," J. Appl. Eng. Sci., vol. 17, no. 3, pp. 311–320, 2019.
5) M. Al-Ghriybah, "Assessment of Wind Energy Potentiality at Ajloun, Jordan Using Weibull Distribution Function," Evergr. Jt. J. Nov. Carbon Resour. Sci. Green Asia Strateg., vol. 09, no. 01, pp. 10–16, 2022.
6) N. Alom, "Influence of curtain plates on the aerodynamic performance of an elliptical bladed Savonius rotor (S-rotor)," Energy Syst., Mar. 2021.
7) Global wind energy council, "Global wind report," 2019.
8) M. Al-ghriybah, M. F. Zulkafli, and D. H. Didane, "Numerical Investigation of Inner Blade Effects on the Conventional Savonius Rotor with External Overlap," J. Sustain. Dev. Energy, Water Environ. Syst., vol. 8, no. 3, pp. 561–576, Sep. 2020.
9) C. Li and K. Ito, "Performance Evaluation of Wind Decontamination System by Computational Fluid Dynamics," Evergreen, vol. 1, no. 2, pp. 12–17, Sep. 2014.
10) A. H. Muheisen, M. A. R. Yass, and I. K. Irthiea, "Enhancement of horizontal wind turbine blade performance using multiple airfoils sections and fences," J. King Saud Univ. - Eng. Sci., Mar. 2021.
11) A. M. Halawa, B. Elhadidi, and S. Yoshida, "Aerodynamic Performance Enhancement Using Active Flow Control on DU96-W-180 Wind Turbine Airfoil," Evergreen, vol. 5, no. 1, pp. 16–24, Mar. 2018.
12) N. A. Ahmed and M. Cameron, "The challenges and possible solutions of horizontal axis wind turbines as a clean energy solution for the future," Renew. Sustain. Energy Rev., vol. 38, pp. 439–460, Oct. 2014.
13) M. Al-Ghriybah, M. F. Zulkafli, D. H. Didane, and S. Mohd, "Performance of the Savonius Wind Rotor with Two Inner Blades at Low Tip Speed Ratio," CFD Lett., vol. 12, no. 3, pp. 11–21, Mar. 2020.
14) S. Toudarbari, M. J. Maghrebi, and A. Hashemzadeh, "Evaluation of Darrieus wind turbine for different highway settings using CFD simulation," Sustain. Energy Technol. Assessments, vol. 45, p. 101077, Jun. 2021.
15) Terence Clinton Rudien et al., "Technical Feasibility Analysis of Wind Energy Potentials in two sites of East Malaysia: Santubong and Kudat," Evergreen, vol. 8, no. 2, pp. 271–279, Jun. 2021.
16) S. Montelpare, V. D'Alessandro, A. Zoppi, and R. Ricci, "Experimental study on a modified Savonius wind rotor for street lighting systems. Analysis of external appendages and elements," Energy, vol. 144, pp. 146–158, Feb. 2018.
17) H. J. Park, S. Yamagishi, S. Osuka, Y. Tasaka, and Y. Murai, "Development of multi-cycle rainbow particle tracking velocimetry improved by particle defocusing technique and an example of its application on twisted Savonius turbine," Exp. Fluids, vol. 62, no. 4, p. 71, Apr. 2021.
18) J. Thiyagaraj, I. Rahamathullah, R. Bharathiraja, G. Anbuchezhiyan, and A. Ponshanmugakumar, "Influence of various augmentation devices on the performance characteristics of modified four bladed fixed flip type savonius hydrokinetic turbine," Mater. Today Proc., vol. 46, pp. 3665–3669, 2021.
19) M. Al-Ghriybah, M. F. Zulkafli, D. H. Didane, and S. Mohd, "Performance of Double Blade Savonius Rotor at Low Rotational Speed," J. Comput. Theor. Nanosci., vol. 17, no. 2, pp. 729–735, Feb. 2020.
20) A. M. Halawa, B. Elhadidi, and S. Yoshida, "POD & MLSM Application on DU96-W180 Wind Turbine Airfoil," Evergreen, vol. 4, no. 1, pp. 36–43, Mar. 2017.
21) M. A. Kamoji, S. B. Kedare, and S. V. Prabhu, "Experimental investigations on single stage, two stage and three stage conventional Savonius rotor," Int. J. Energy Res., vol. 32, no. 10, pp. 877–895, Aug. 2008.
22) T. Hayashi, Y. LI, and Y. HARA, "Wind Tunnel Tests on a Different Phase Three-Stage Savonius Rotor," JSME Int. J. Ser. B, vol. 48, no. 1, pp. 9–16, 2005.
23) N. H. Mahmoud, A. A. El-Haroun, E. Wahba, and M. H. Nasef, "An experimental study on improvement of Savonius rotor performance," Alexandria Eng. J., vol. 51, no. 1, pp. 19–25, Mar. 2012.
24) V. J. Modi, N. J. Roth, and M. S. U. K. Fernando, "Optimum-configuration studies and prototype design of a wind-energy-operated irrigation system," J. Wind Eng. Ind. Aerodyn., vol. 16, no. 1, pp. 85–96, Jan. 1984.

25) K. S. Jeon, J. I. Jeong, J.-K. Pan, and K.-W. Ryu, “Effects of end plates with various shapes and sizes on helical Savonius wind turbines,” Renew. Energy, vol. 79, pp. 167–176, Jul. 2015.
26) M. Al-Ghriybah, M. F. Zulkafli, D. H. Didane, and S. Mohd, “Review of the Recent Power AugmentationTechniquesfor the Savonius Wind Turbines,” J. Adv. Res. Fluid Mech. Therm. Sci., vol. 60, no. 1, pp. 71–84, 2019.
27) J. V. Akwa, G. Alves da Silva Júnior, and A. P. Petry, “Discussion on the verification of the overlap ratio influence on performance coefficients of a Savonius wind rotor using computational fluid dynamics,” Renew. Energy, vol. 38, no. 1, pp. 141–149, Feb. 2012.
28) M. Al-Ghriybah, M. Fadhli Zulkafli, D. Hissein Didane, and S. Mohd, “The effect of spacing between inner blades on the performance of the Savonius wind turbine,” Sustain. Energy Technol. Assessments, vol. 43, p. 100988, Feb. 2021.
29) M. Al-Ghriybah, M. F. Zulkafli, D. H. Didane, and S. Mohd, “The effect of inner blade position on the performance of the Savonius rotor,” Sustain. Energy Technol. Assessments, vol. 36, p. 100534, Dec. 2019.
30) I. Ushiyama, H. NAGAI, and J. SHINODA, “Experimentally Determining the Optimum Design Configuration for Savonius Rotors,” Bull. JSME, vol. 29, no. 258, pp. 4130–4138, 1986.
31) H. R. Rahai, “Development of optimum design configuration and performancefor vertical axis wind turbine: feasibility analysis andfinal EISG report 2005.,” USA, 2015.
32) A. Banerjee, S. Roy, P. Mukherjee, and U. K. Saha, “Unsteady Flow Analysis Around an Elliptic-Bladed Savonius-Style Wind Turbine,” in ASME 2014 Gas Turbine India Conference, 2014.
33) S. Roy and U. K. Saha, “Numerical Investigation to Assess an Optimal Blade Profile for the Drag Based Vertical Axis Wind Turbine,” in Volume 6A: Energy, 2013.
34) S. Roy, P. Mukherjee, and U. K. Saha, “Aerodynamic Performance Evaluation of a Novel Savonius-Style Wind Turbine Under an Oriented Jet,” in ASME 2014 Gas Turbine India Conference, 2014.
35) U. K. Saha, S. Thotla, and D. Maity, “Optimum design configuration of Savonius rotor through wind tunnel experiments,” J. Wind Eng. Ind. Aerodyn., vol. 96, no. 8–9, pp. 1359–1375, Aug. 2008.
36) B. Zhang, B. Song, Z. Mao, and W. Tian, “A novel wake energy reuse method to optimize the layout for Savonius-type vertical axis wind turbines,” Energy, vol. 121, pp. 341–355, Feb. 2017.2)
37) D. H. Didane, N. Rosly, M. F. Zulkafli, and S. S. Shamsudin, “Numerical investigation of a novel contra-rotating vertical axis wind turbine,” Sustain. Energy Technol. Assessments, vol. 31, pp. 43–53, Feb. 2019.
38) M. Mosbahi et al., “Performance improvement of a Savonius water rotor with novel blade shapes,” Ocean Eng., vol. 237, p. 109611, Oct. 202.